A Unified Framework for Surface Flux-Driven Cyclones Outside the Tropics

1. Introduction

Cyclones with structures very similar to those of tropical cyclones are occasionally observed to develop well outside the tropics. These include polar lows (global high latitudes), medicanes (Mediterranean and Black Seas), subtropical cyclones (North Atlantic), and Kona Storms (central North Pacific). The identification of such systems is usually based on their appearance in satellite imagery and, to some extent, on the environmental conditions in which they occur. Here we claim that many of these systems are manifestations of the same physical phenomenon and, as such, should be given a common, physically-based designation. We propose to call these "X-cyclones"[1].

Cyclones of synoptic and sub-synoptic scale are powered by one or both of two energy sources: the available potential energy (APE) associated with isobaric temperature gradients (baroclinity), and fluxes of enthalpy (sensible and latent heat) from the ocean to the atmosphere. A normal extratropical cyclone over land is an example of the former, while the latter is epitomized by a classical tropical cyclone. Extratropical transitioning and hybrid cyclones are powered by both sources, with the relative proportion usually varying over the life of the storm. We note that tropical cyclones often originate in disturbances, such as African easterly waves, that derive their energy from isobaric temperature gradients.

We assert that, like tropical cyclones, X-cyclones are powered by surface enthalpy fluxes, but differ from the former in that the required thermodynamic potential is produced locally and transiently by baroclinic processes, whereas thermodynamic potential is always present in the seasons and regions where tropical cyclones develop. And, like tropical cyclones, they are often triggered by baroclinic processes.

In the following sections we present case studies of the development of medicanes, polar lows, a subtropical cyclone, and a Kona Storm, showing that the dynamic and thermodynamic pathways are similar. Specifically, each case developed after the formation of a deep, cold-core cut-off cyclone in the upper troposphere that often resulted from a Rossby wave breaking event. The lifting of the tropospheric air in response to the developing potential vorticity anomaly near the tropopause creates a deep, cold, nearly saturated column. The deep cold air over bodies of water substantially elevates potential intensity, while its high relative humidity discourages convective downdrafts, which tamp down the needed increase in boundary layer enthalpy. Low

[1] "X" is a placeholder here. Some ideas: "Surface Flux Assisted Cyclones (SFACs)"; "CYClones from Locally Originating Potential intensity (CYCLOPs)"

shear near the core of the cutoff cyclone, coupled with high potential intensity and humidity, provide an ideal embryo for tropical cyclone development.

Yet, as is the case with tropical cyclones, there are variations on the theme, and we explore these in the closing sections.

2. Why it matters

Why should we care whether a cyclone is driven by surface fluxes or baroclinity? From a practical forecasting standpoint, the distributions of weather hazards, like rain and wind, can be very different, as can be the development time scales and fundamental predictability.

In classical baroclinic cyclones, the strongest winds are often found in frontal zones and can be far from the cyclone center, and precipitation is usually heaviest in these frontal zones and in a shield of slantwise ascent extending poleward from the surface cyclone. There is long experience in forecasting baroclinic storms, and today's numerical weather prediction (NWP) of these events has become quite accurate, even many days ahead. Importantly, baroclinic cyclones are well resolved by today's NWP models. While baroclinic cyclones can intensify rapidly, both the magnitude and timing of intensification are usually forecast accurately, and uncertainties are well quantified by NWP ensembles.

By contrast, the physics of tropical cyclone intensification, involving a positive feedback between surface winds and surface enthalpy fluxes, results in an intense, concentrated core with high winds and heavy precipitation (which can be snow in the case of polar lows). The eyewalls of surface flux-driven cyclones are strongly frontogenetical, further concentrating wind and rain in an annulus of mesoscale dimensions. The intensity of flux-driven cyclones can change very rapidly and often unpredictably, presenting a severe challenge to forecasters. For example, Hurricane Otis of 2023 intensified from a tropical storm to a Cat 5 hurricane in about 30 hours, devastating Acapulco, Mexico, with little warning from forecasters. The small size of the core of high winds and heavy precipitation means that small errors in the forecast position of the storm lead to large errors in local wind and precipitation. Flux-driven cyclones are too small to be well resolved by today's global NWP models, and even if they were, fundamental predictability studies show high levels of intrinsic unpredictability of rapid intensity changes.

The time and space scales of surface flux-driven cyclones are such that they couple strongly with the ocean, producing near-inertial currents whose shear-driven turbulence mixes to the surface generally (but not always) colder water from below the surface mixed layer. This has an important (usually negative) feedback on the intensity of such cyclones. Accurate numerical forecasting of surface flux-driven cyclones therefore requires an interactive ocean, generally missing from today's NWP models because it is not very important for baroclinic cyclones.

For these reasons, it matters (or should matter) to forecasters whether a particular development is primarily driven by surface fluxes or by ambient baroclinity. The structural differences described above are often, but not always, detectable in satellite imagery; at the same time, such imagery is sometimes misleading about the underlying physics. For example, classical baroclinic development sometimes develops cloud-free eyes surrounded by convection, through

the warm occlusion process, even over land, and yet may not have the intense annular concentration of wind and rain characteristic of surface flux-driven cyclones.

We next present examples of X-cyclones in many extratropical regions.

3. Case Studies

a. Medicane of January, 1995

On average, two medicanes are observed annually in the Mediterranean and Black Seas. We begin with a system, Medicane Celeno, that reached maturity on 16 January, 1995, shown in infrared satellite imagery in Figure 1.

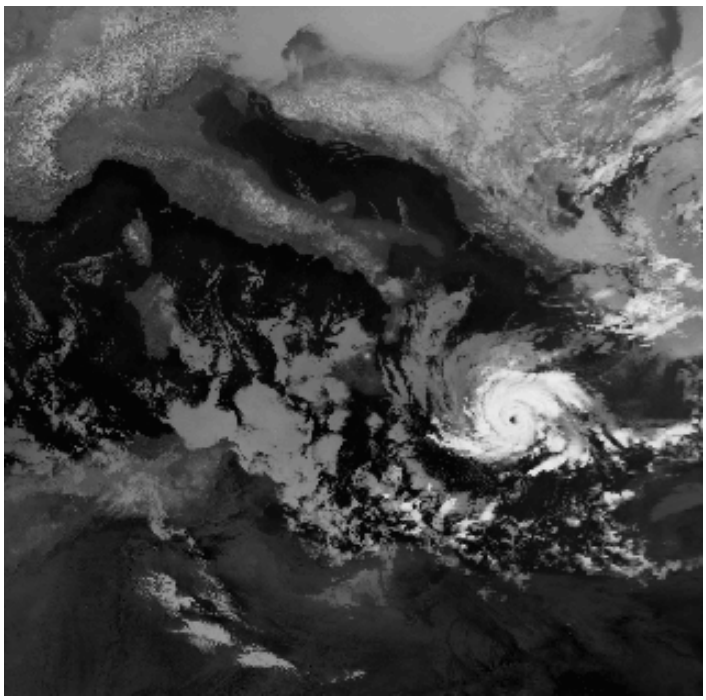

Figure 1: Infrared satellite image of Medicane Celeno in the central Mediterannean, at 09:06 UTC 16 January 1995.

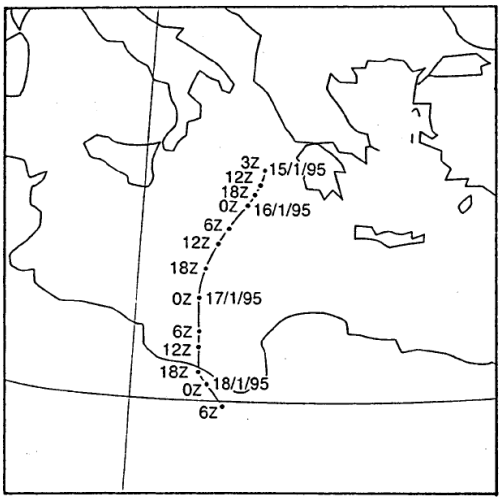

Figure 2: Track of the surface center of the cyclone between 03:00 UTC on January 15 and 06:00 on January 18, 1995, derived from satellite images.

Figure 2 shows the track of the surface center of the cyclone, which developed between Greece and Sicily and made landfall in Libya. A detailed description of this medicane is provided by Pytharoulis et al. (1999).

The evolution of the system in increments of 24 hours, beginning on 00 GMT, 12 January and ending at 00 GMT 15 January, is shown in Figure 3. This sequence covers the period just before the system develops and shows the 400 hPa and 950 hPa geopotential heights. The evolution of the upper tropospheric (400 hPa) height field shows a classic Rossby wave breaking event (McIntyre and Palmer 1983) in which an eastward-moving baroclinic Rossby wave at higher latitudes amplifies and irreversibly breaks to the south and west, finally forming a cut-off cyclone. As the cold pool is gradually heated by the underlying sea, a broad surface cyclone develops by 00 GMT on January 14th. At around this time, the feedback between surface wind and surface enthalpy fluxes is strong enough to develop a tight inner warm core (warm, that is, relative to the surrounding cold pool, not necessarily to the unperturbed larger scale environment) by 00 GMT on January 15th. At the same time, the upper cold core weakens, no doubt aided by the strong heating from the surface transferred aloft by deep convection.

An important aspect of the physics of this development is conveyed by Figure 4, which shows the corresponding evolutions of the contribution to a genesis potential index (GPI) of the tropical cyclone potential intensity (Emanuel 1986; Bister and Emanuel 2002) and mid-tropospheric (600 hPa) relative humidity. The contribution of potential intensity to GPI (Emanuel 2010) is here defined as

$$GPI_{V_{pot}} \equiv 0.001*(\mathrm{MAX}(V_{pot} - 35\,ms^{-1}, 0))^2, \quad (1)$$

where V_{pot} is the potential intensity in ms^{-1}. Note that the leading multiplicative factor is arbitrary. Both potential intensity and mid-tropospheric humidity play key roles in empirical tropical cyclone genesis indices.

Referring to Figure 4, note that the $GPI_{V_{pot}}$ is essentially zero on January 12th, 3 days before the development, but as the cold cyclone develops aloft, it increases rather substantially. This is what distinguishes X-cyclones from tropical cyclones: In the latter case the potential intensity is always large over the seasons and warm-pool regions where they develop, whereas X-cyclones rely on local deep tropospheric cooling to produce the needed thermodynamic potential on the synoptic scale.

Notice that there is a local minimum in $GPI_{V_{pot}}$ where the medicane develops west of Peloponnese in December 15th. This is an artifact of the way potential intensity is calculated, which assumes that the ocean and atmosphere above it represent the environment of a tropical cyclone or X-cyclone. In the core of a well-developed surface flux-driven cyclone, the eye and eyewall can be close to thermodynamic equilibrium with the sea, so that locally, a sample of air lifted from a state of saturation at sea surface pressure and temperature can have the same virtual temperature of the surrounding air. Indeed, a TC at its potential intensity will have zero measured potential intensity in its core.

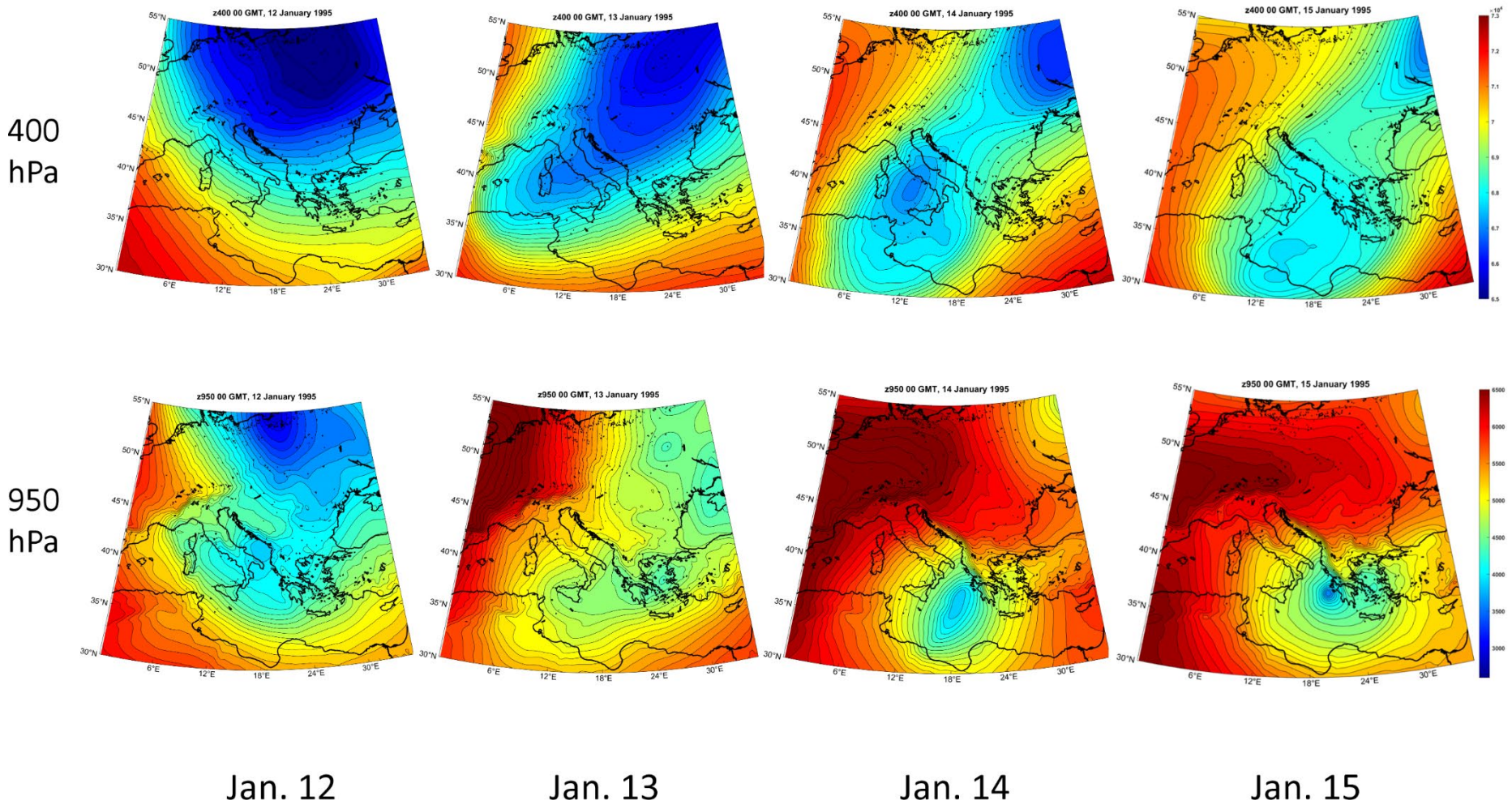

Figure 3: Evolution of the 400 hPa (top) and 950 hPa (bottom) geopotential heights in 24-hour increments, from 00 GMT 12 January to 00 GMT 15 January, 1995. These fields are from ERA5 reanalyses.

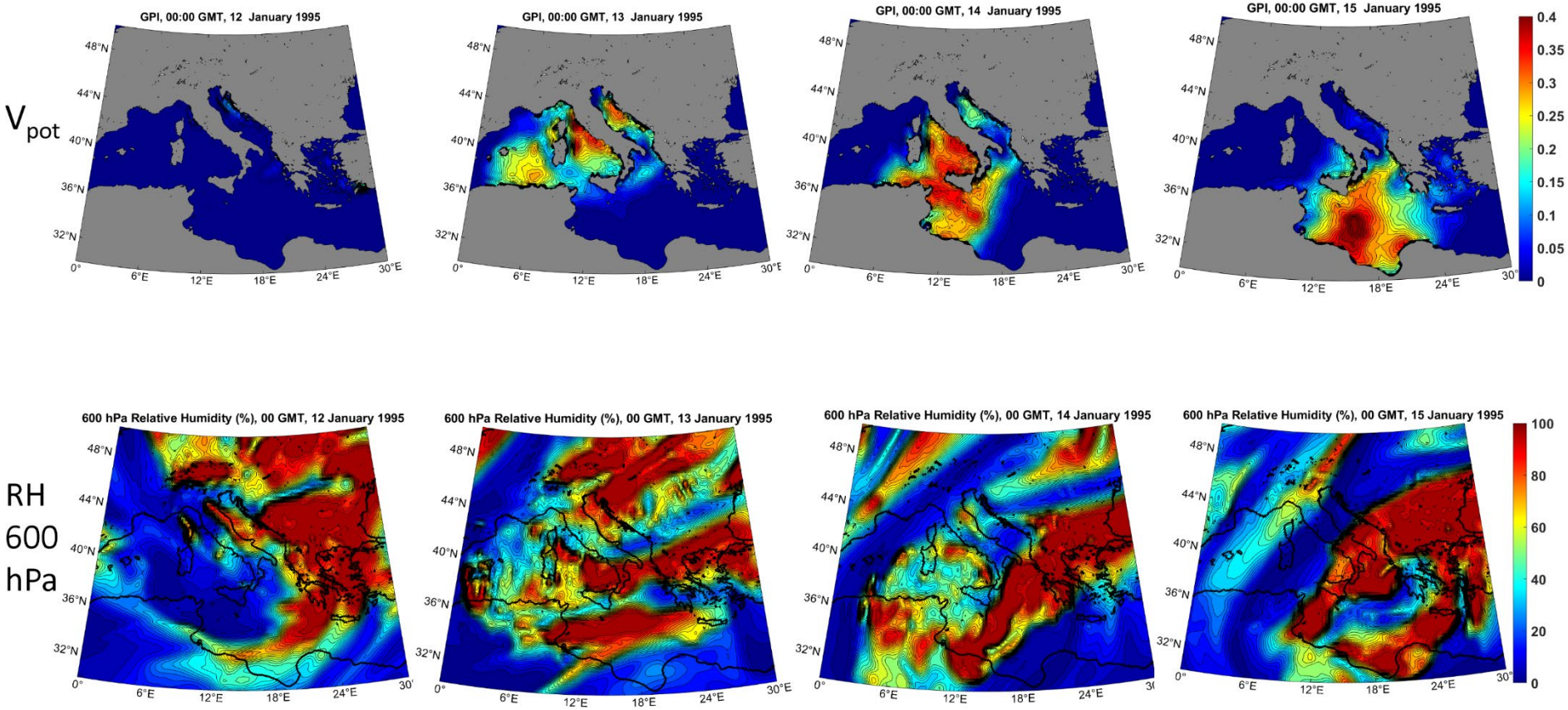

Figure 4: Evolution of the genesis index contribution from potential intensity (top) and 600 hPa relative humidity (bottom) for the same times as those shown in Figure 3.

The evolution of humidity in the middle troposphere (600 hPa; second row of Figure 4) is more complex, with bands of high humidity alternating with dry tongues of air. In principle, X-cyclones, like their tropical cousins, should have nearly saturated cores, but it is not clear that such cores are captured by reanalyses, given the paucity of observations over the ocean. We will address this problem in the next subsection.

b. Medicane of December 2005

An unnamed medicane formed on December 14th 2005 off the coast of Tunisia and then moved eastward across a large stretch of the Mediterranean. Figure 5 shows a satellite image of this medicane on December 15th. This cyclone has been the subject of several intensive studies (e.g. Fita and Flaounas 2018; Miglietta et al. 2021).

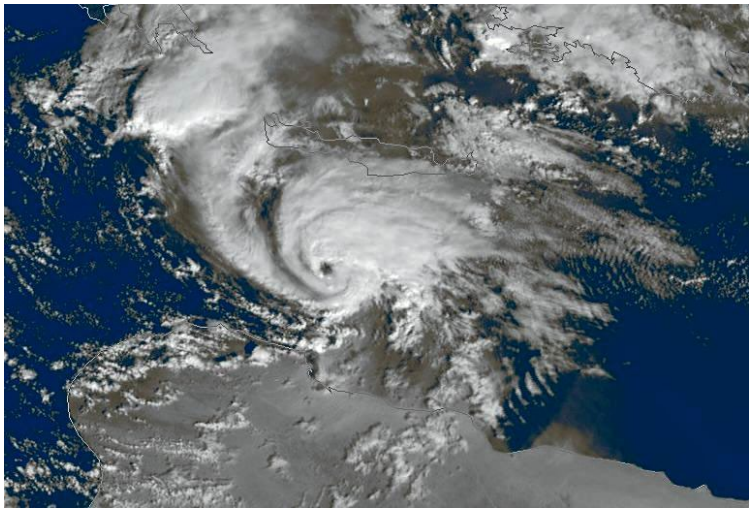

Figure 5: Medicane between Crete and Libya on 15 December 2005.

Like Medicane Celeno, it formed as a result of a Rossby wave breaking event, as illustrated in Figure 6. On December 8th (panel a), a deep trough is digging southward over eastern Europe, but by the 9th (panel b) has split in two, with the westward half breaking southwestward over Germany and Switzerland. By the 11th (panel d), this local minimum is located over Tunisia and on the 12th (panel e) is more or less completely cut off from the main westerly jet. It subsequently oscillates over Tunisia and Algeria, before moving slowly eastward over the Mediterranean, as shown in Figure 7.

As the cut-off cyclone in the upper troposphere and associated cold pool move off the coast of Tunisia, the medicane rapidly develops just offshore and moves eastward with the cut-off low, reaching peak intensity early on the 15th, though the ERA5 reanalysis has it stronger on the 14th (lower panels of Figure 7). This medicane develops as the cut-off low is slowly being re-absorbed into the westerlies. It continues eastward and dissipates in the far eastern Mediterranean on the 16th (not shown).

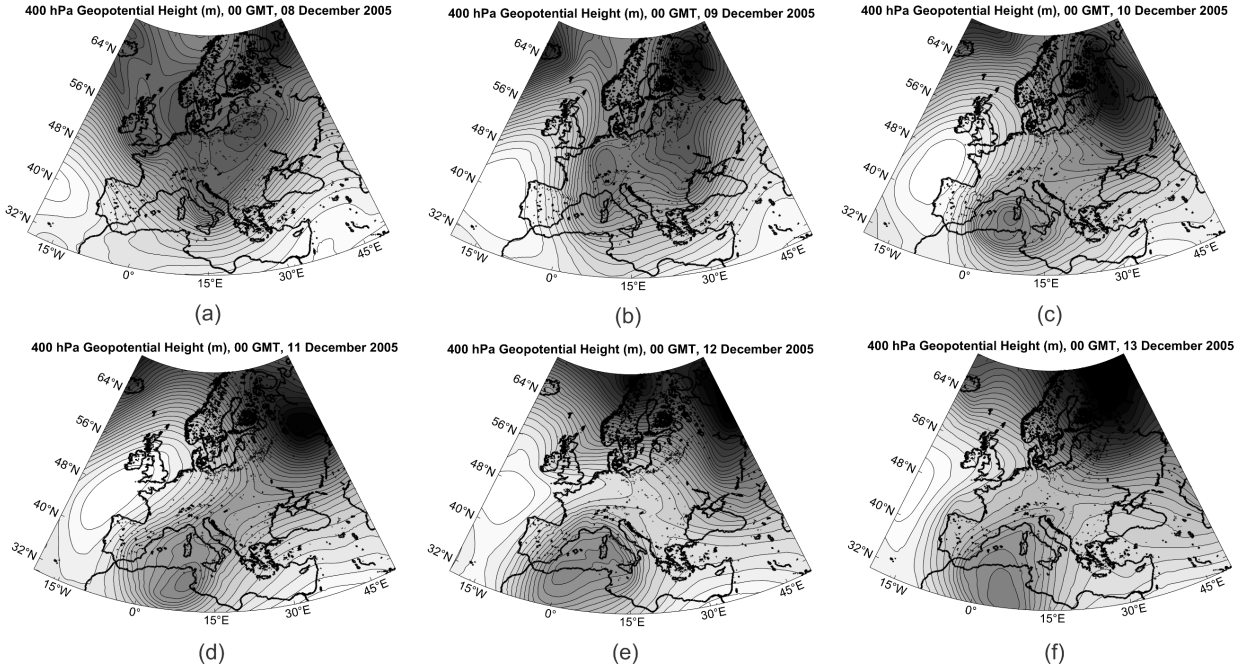

Figure 6: 400 hPa heights, ranging from 6.5 km to 7.3 km (gray scale identical for all panels) at 00 GMT on December 8th (a), 9th (b), 10th (c), 11th (d), 12th (e), and 13th (f), 2005. From ERA-5 reanalyses.

The evolutions of $GPI_{V_{pot}}$ as given by (1) and 600 hPa relative humidity on the 14th and 15th of December are shown in Figure 8. In this case, there were large meridional gradients of sea surface temperature across the Mediterranean, ranging from over 20ºC in the far south to less than 12ºC in the northern reaches of the Adriatic and western Mediterranean (not shown here). As the cold pool moved southwestward and deepened, little or no $GPI_{V_{pot}}$ developed over the northern Mediterranean, but beginning on December 10th, larger values develop over the Gulf of Sidra, east of Tunisia. On the 14th, the development of a strong warm core surface system artificially suppressed the calculated $GPI_{V_{pot}}$ near the cyclone center, as evident in Figure 8a, and this suppression continued on the 15th (Figure 8b). This artificial suppression aside, the movement of the cold pool over the warm waters of the Gulf of Sidra clearly gave rise to substantial thermodynamic potential for X-cyclones.

As with Medicane Celeno, the mid-tropospheric relative humidity field was complex near the cyclone core (Figure 8c) but by the 15th the core air appeared to be nearly saturated (Figure 8d). In this case, total column water vapor from satellite microwave and near infrared images (Schröder et al. 2023) was available for December 14th (Figure 9) and can be compared with the 600 hPa relative humidity (Figure 8c). Though somewhat coarser in resolution, the observed total column water vapor does suggest that the core of this medicane might have been close to saturation at this time, and suggests that the fine structure of mid-tropospheric humidity in reanalyses might not be very reliable.

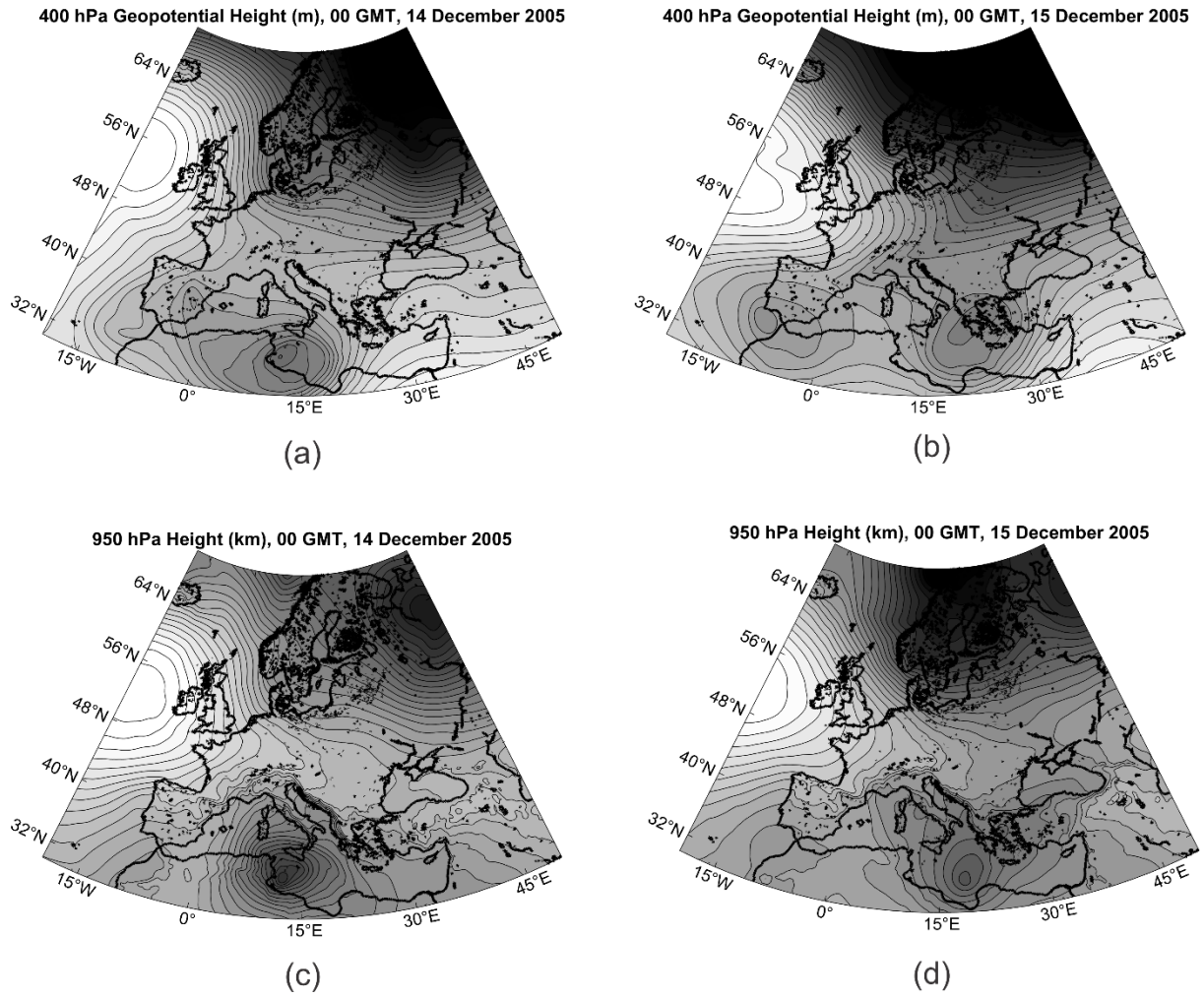

Figure 7: Evolution of 400 hPa height, ranging from 6.5 to 7.3 km (a and b), and 950 hPa height, ranging from 250 to 750 m (c and d) at 00 GMT in December 14th (left) and 15th (right), 2005. The gray scales of (a) and (b) are identical, as are the gray scales of (c) and (d). From ERA-5 reanalyses.

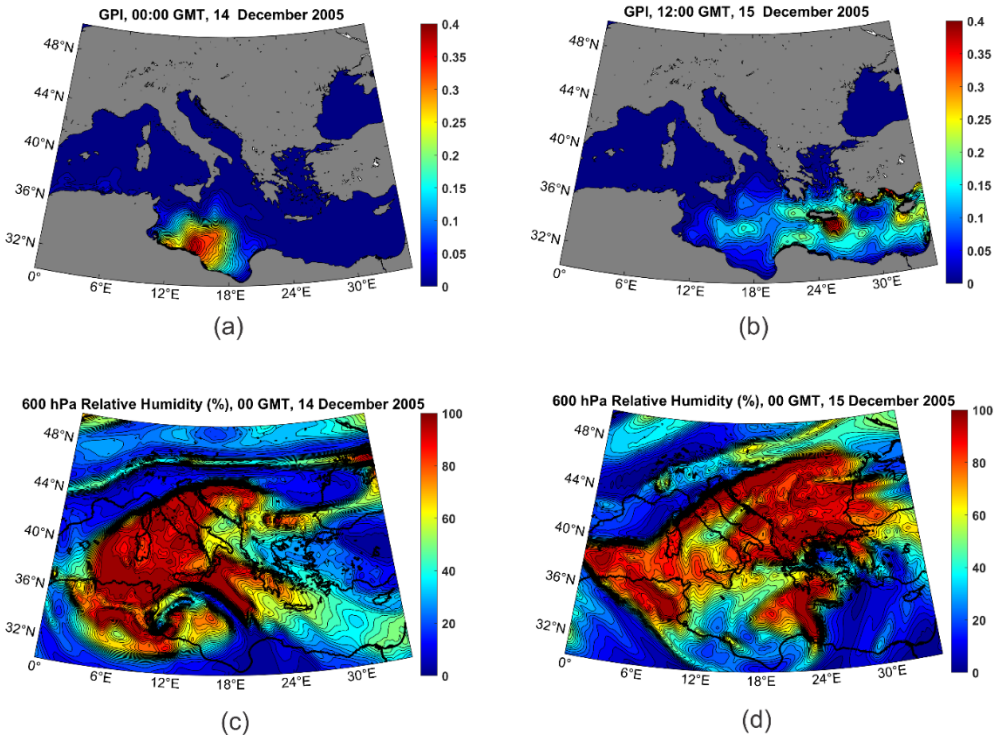

Figure 8: Potential intensity contribution to the GPI (a and b) and 600 hPa relative humidity (c and d) at 00 GMT on December 14th (left) and 15th (right). Color scales are the same as those in Figure 4. From ERA-5 reanalyses.

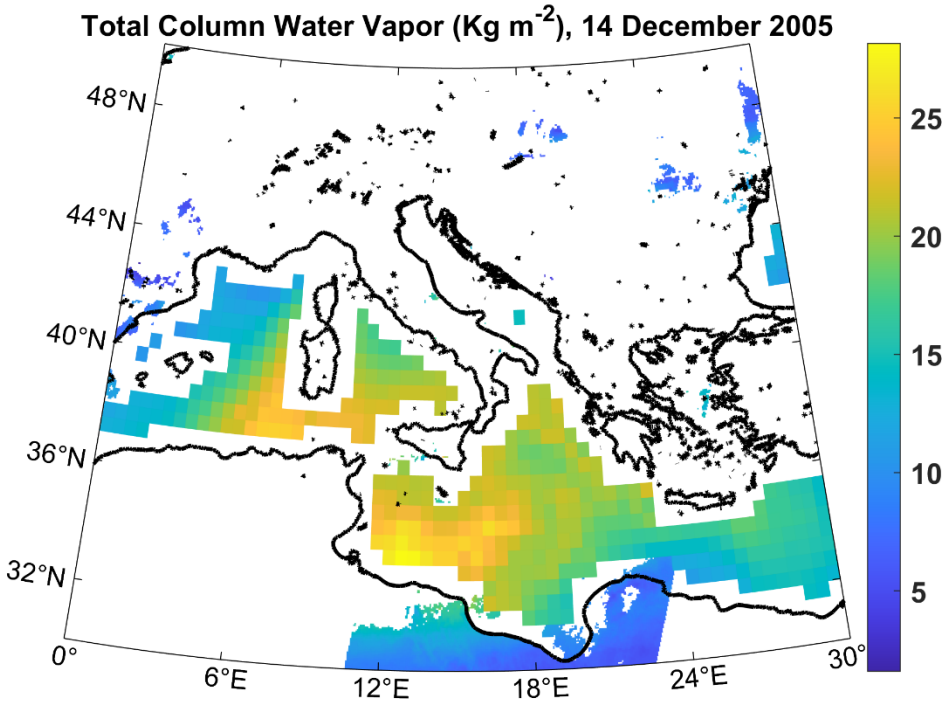

Figure 9: Total column water vapor (Kg m^{-2}) at 00 GMT on 14 December 2005, derived from microwave and near infrared imagers.

c. Polar low of February, 1987

Closed upper tropospheric lows also provide favorable environments for X-cyclone developments at very high latitudes in locations where there is open water. These usually form poleward of the mid-latitude jet, where quasi-balanced dynamics can be quite different. Figure 10 in an infrared image of a polar low that formed just south of Svalbard on February 25th, 1987, and tracked southward, making landfall on the north coast of Norway on the 27th. This system was studied extensively by Nordeng and Rasmussen (1992).

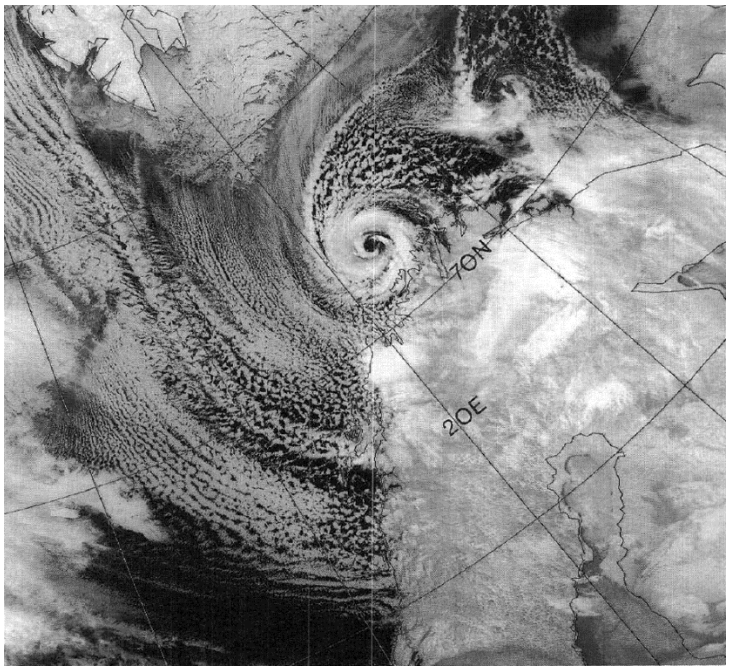

Figure 10: NOAA 9 satellite infrared image (channel 4) of a polar low just north of Norway at 08:31 GMT on 27 February 1987.

As with medicanes, polar lows develop in strongly convecting air masses when cold air moves out over relatively warm water. The adjective “relatively” is crucial here; with polar lows the sea surface temperature is often only marginally above the freezing point of saltwater. Figure 11 shows the distribution of sea surface temperature on February 25th, with the uniform dark blue areas denoting regions of sea ice cover. The polar low shown in Figure 10 develops when deep cold air moves southward over open water, as shown in Figure 12.

In this case, it is not clear whether one can describe what happens in the upper troposphere (top row of Figure 12) as a Rossby wave breaking event. Instead, what we see here is a complex rearrangement of the tropospheric winter polar vortex, as a ridge building over North America breaks and forms an anticyclone over the North Pole. This complex rearrangement results in the formation of a deep cutoff low just south of Svalbard by the 26th, which then moves southward over Norway by the 27th. The polar low is barely visible in the 950 hPa height field on the 25th (middle row of Figure 12), but intensifies rapidly as it moves over progressively warmer water, reaching maturity before landfall on the 27th.

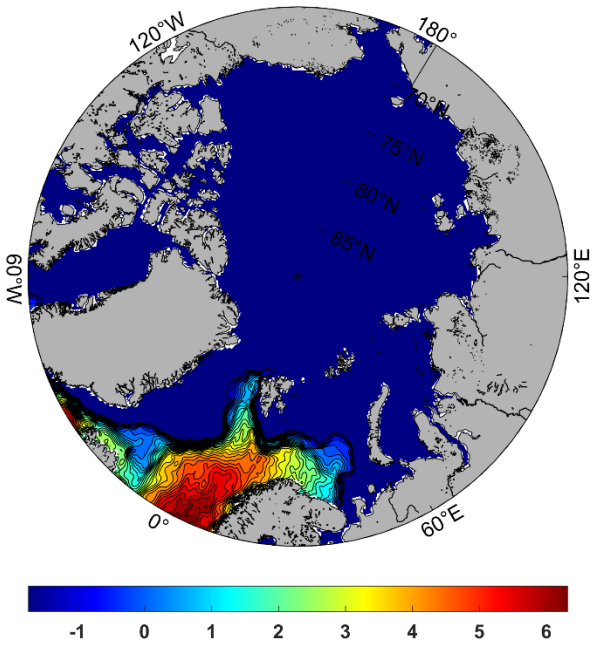

Figure 11: Sea surface temperature (°C) at 02:00 GMT on 25 February, 1987, from ERA5 reanalysis. Dark blue areas denote regions of sea ice. From ERA-5 reanalyses.

The evolution of the $GPI_{V_{pot}}$ field is shown in the bottom row of Figure 12. Here, for clarity, we have lowered the threshold potential intensity that appears in (1) from $35\,ms^{-1}$ to $30\,ms^{-1}$. (We do not display the relative humidity here because at these very low temperatures, the field is not very relevant to the physics.) The thermodynamic potential for X-cyclones develops rapidly south of Svalbard as the cut-off cyclone moves out over open water. The bullseye minimum evident in the rightmost panel is owing to the aforementioned artificial effect of the X-cyclone itself on the calculation of potential intensity, and likely masks the true maximum of potential intensity at this location.

Under these conditions, almost all the surface flux that drives the X-cyclone is in the form of sensible, rather than latent, heating, and the background state has a nearly dry (rather than moist) adiabatic lapse rate. As shown by Cronin and Chavas (2019) and Velez-Pardo and Cronin (2023), surface flux-driven cyclones can develop in perfectly dry convecting environments, though they generally reach smaller fractions of their potential intensity and lack the long tail of the radial profile of azimuthal winds that is a consequence of the dry stratification resulting from background moist convection (Chavas and Emanuel 2014). They also have larger eyes relative to their overall diameters.

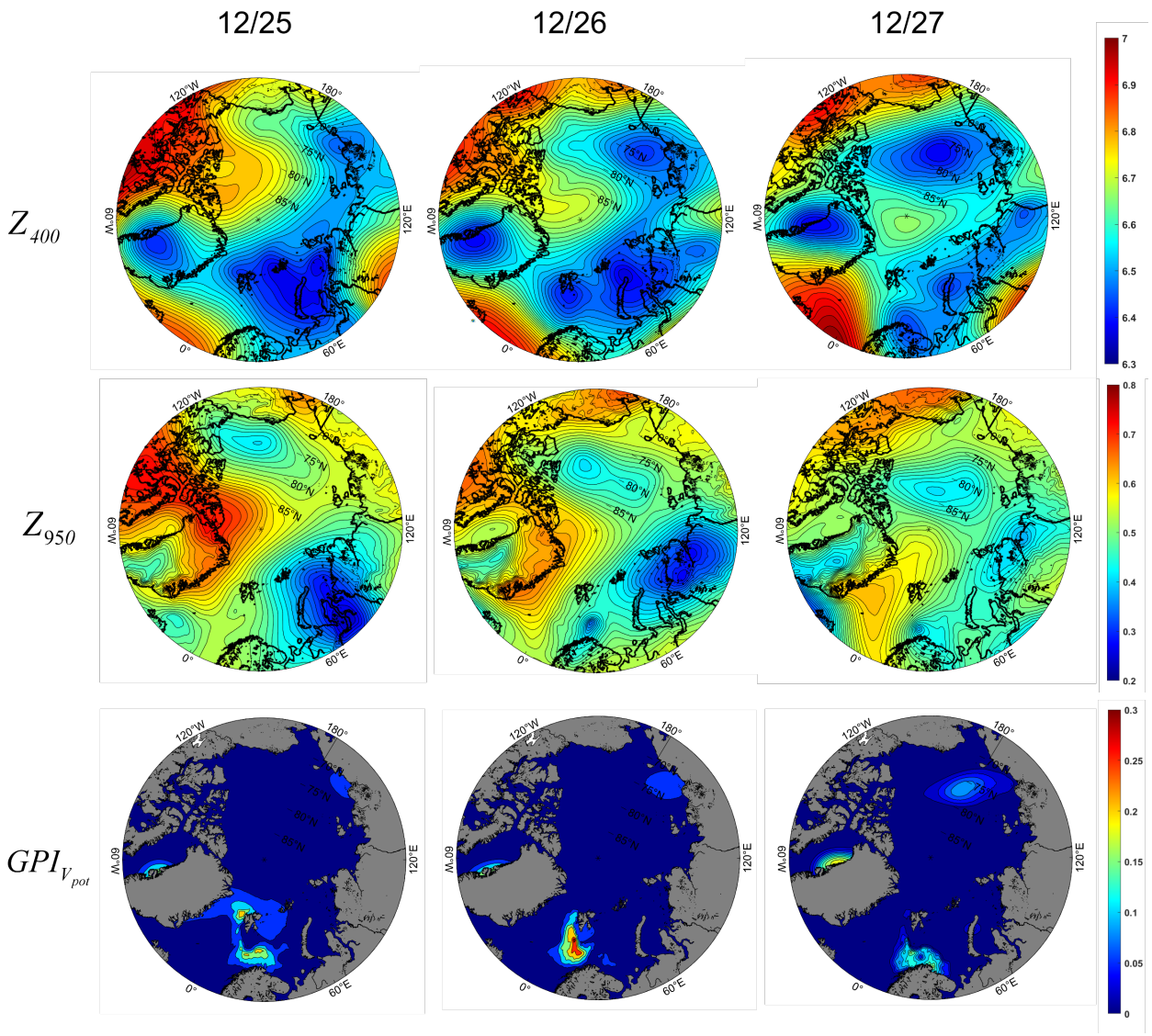

Figure 12: 400 hPa geopotential height (km; top), 950 hPa geopotential height (km; middle), and $GPI_{V_{pot}}$ (bottom), at 02:00 GMT on February 25th (left), 26th (center), and 27th (right), 1987. From ERA-5 reanalyses.

One interesting feature of polar waters in winter is that the thermal stratification is sometimes reversed from normal, with warmer waters lying beneath cold surface waters. This is made possible, in part, by strong salinity stratification, that keeps the cold water from mixing with the warmer waters below. Also, seawater has maximum density around 4°C and colder waters are therefore lighter and stay at the surface. Therefore, it is possible for polar lows to generate warm, rather than cold, wakes, and this feeds back positively on their intensity. This seems to happen in roughly half the documented cases of polar lows in the Nordic seas (Tomita and Tanaka 2024).

d. Polar low over the Sea of Japan, December, 2009

Polar lows are not uncommon in the Sea of Japan, forming when deep, cold air masses from Eurasia flow out over relatively warm ocean. They are frequent enough to warrant a climatology (Yanase and co-authors 2016). A satellite image of one such storm is shown in Figure 13.

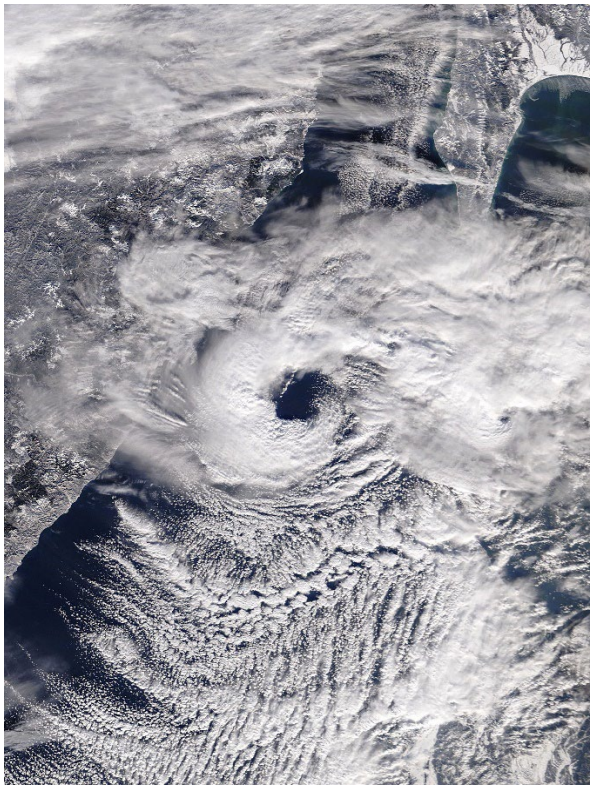

Figure 13: Polar low over the northern Sea of Japan, 02:13 GMT 20 December, 2009 as captured by the MODIS imager on NASA's Terra satellite.

The cyclone traveled almost due south from this point, striking the Hokkaido region of Japan, near Sapporo, with gale-force winds and heavy snow. As with other X-cyclones, it formed in an environment of deep convection under a cold low aloft.

The development of the cutoff cyclone aloft was complex, as shown by the sequence of 400 hPa maps displayed in Figure 14. These are 00 GMT charts at 1-day intervals beginning on December 11th and ending on the 20th, about the time of the image in Figure 13. A large polar vortex is centered in northern central Russia on the 11th but sheds a child low southeastward on the 12th and 13th, becoming almost completely cutoff on the 14th. The parent low drifts westward during this time. The newly formed cutoff cyclone meanders around in isolation from the 15th through the 17th, but becomes wrapped up with a system propagating in to the domain from the east on the 18th. By the 20th, a small-scale cutoff cyclone is drifting southward over the northern Sea of Japan, and it is this upper cutoff that spawns the polar low.

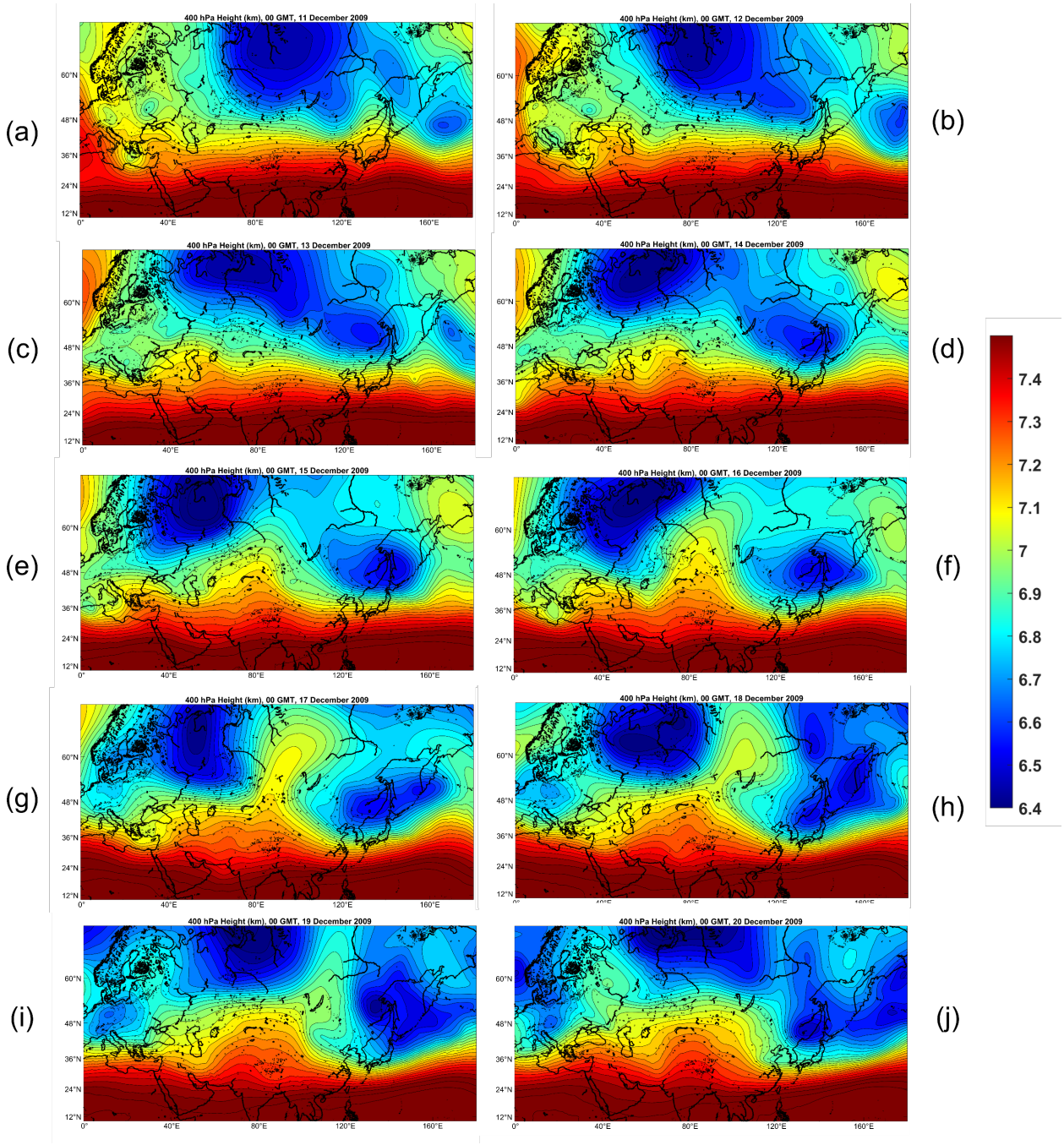

Figure 14: Sequence of 400 hPa geopotential height (km) charts at 1-day intervals from 00 GMT on December 11th (a) to 00 GMT on December 20th (j). The charts span from 0º to 180º longitude and from 10º to 70º latitude. From ERA-5 reanalyses.

The 950 hPa height field and the $GPI_{V_{pot}}$ field at 00 GMT on December 20th are shown in Figure 15. As with the previous polar low case, the $GPI_{V_{pot}}$ uses a threshold of 30 ms^{-1}. At this time, the surface low is developing rapidly and moving southward into a region of high thermodynamic potential. The latter reaches a maximum near the northwest coast of Japan, where the sea surface temperatures are larger. As with the two medicane cases and the other polar low case, the X-cyclone develops in a place where there is normally little or no thermodynamic potential for surface flux-driven cyclones but for which the required thermodynamic potential is created by the approach of a deep cold cyclone aloft.

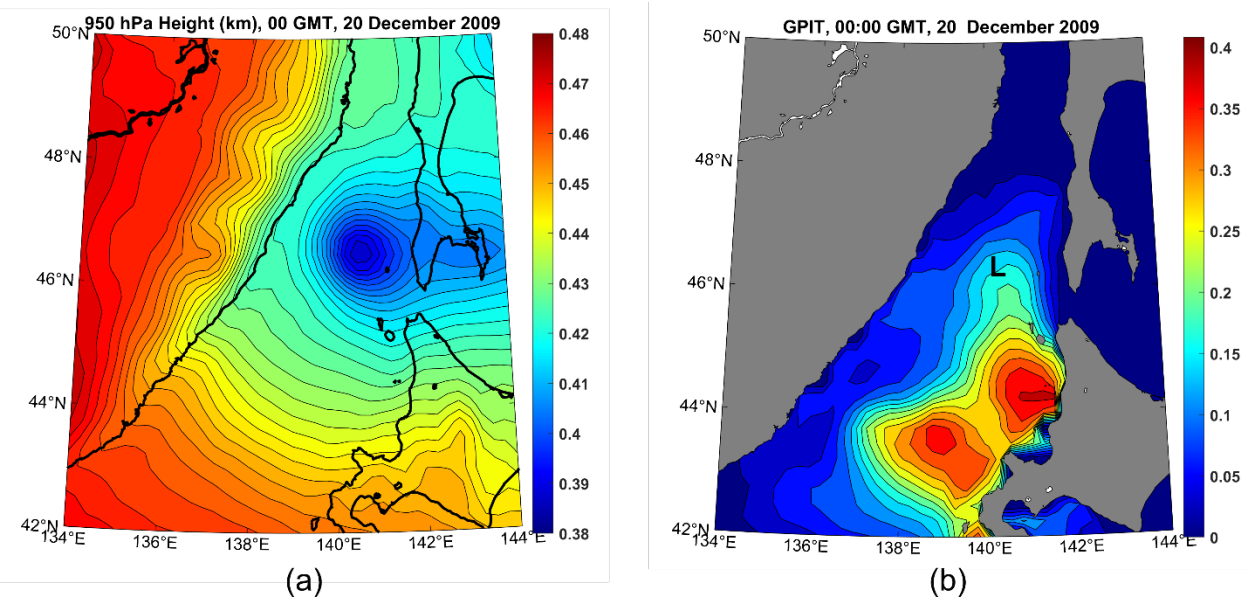

Figure 15: 950 hPa geopotential height (a; km) and $GPI_{V_{pot}}$ (b) at 00 GMT on 20 December, 200. In (b), the "L" marks the satellite-derived surface cyclone center. From ERA-5 reanalyses.

e. The subtropical cyclone of January, 2023

The term "subtropical cyclone" has been used to describe a variety of cyclonic storms in the North Atlantic that do not cleanly meet the definition of a tropical cyclone. Here we will use the term to designate X-cyclones in the North Atlantic; that is, surface flux-powered cyclones that develop in regions and times whose climatological thermodynamic potential is small or zero. This usage may not be consistent with other definitions. The point here is to show that X-cyclones can occur in the North Atlantic and we can safely refer to these as X-cyclones whether or not they meet some definition of "subtropical cyclone".

Figure 16 displays a visible satellite image of a subtropical cyclone over the western North Atlantic on 16 January, 2023. It resembles the medicanes and polar lows described previously, and like them, formed under a cutoff cyclone aloft.

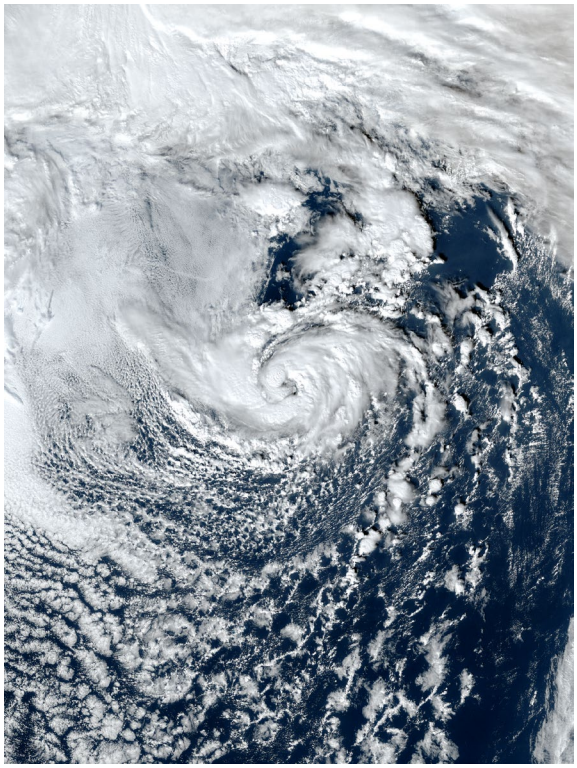

Figure 16: Subtropical cyclone over the western North Atlantic, 18:20 GMT, 16 January 2023.

The formation of the cutoff cyclone aloft is shown in Figure 17. A deep trough advances slowly eastward over eastern North America and partially cuts off on the 14th. As the associated cold pool and region of light shear migrate out over the warm waters south of the Gulf Stream, an X-cyclone forms and intensifies with peak winds of around 60 kts at around 00 GMT on the 17th (Cangliosi et al. 2023). Note also the anticyclonic wave breaking event to the east of the surface cyclone development.

The evolution of the surface cyclone and associated $GPI_{V_{pot}}$ field is displayed in Figure 18. (Note that this figures zooms in to the developing surface cyclone, compared to Figure 17.) On January 14th, the only non-zero values of $GPI_{V_{pot}}$ are in the Gulf Stream and in the far southwestern portion of the domain. The 950 hPa height field shows a broad trough associated with the baroclinic wave moving slowly eastward off the U.S. east coast. But as the upper cold cyclone moves out over warmer water on the 15th, positive $GPI_{V_{pot}}$ develops south of the Gulf Stream, and a closed and more intense surface cyclone develops under the lowest 400 hPa heights and over the region of intensifying $GPI_{V_{pot}}$.

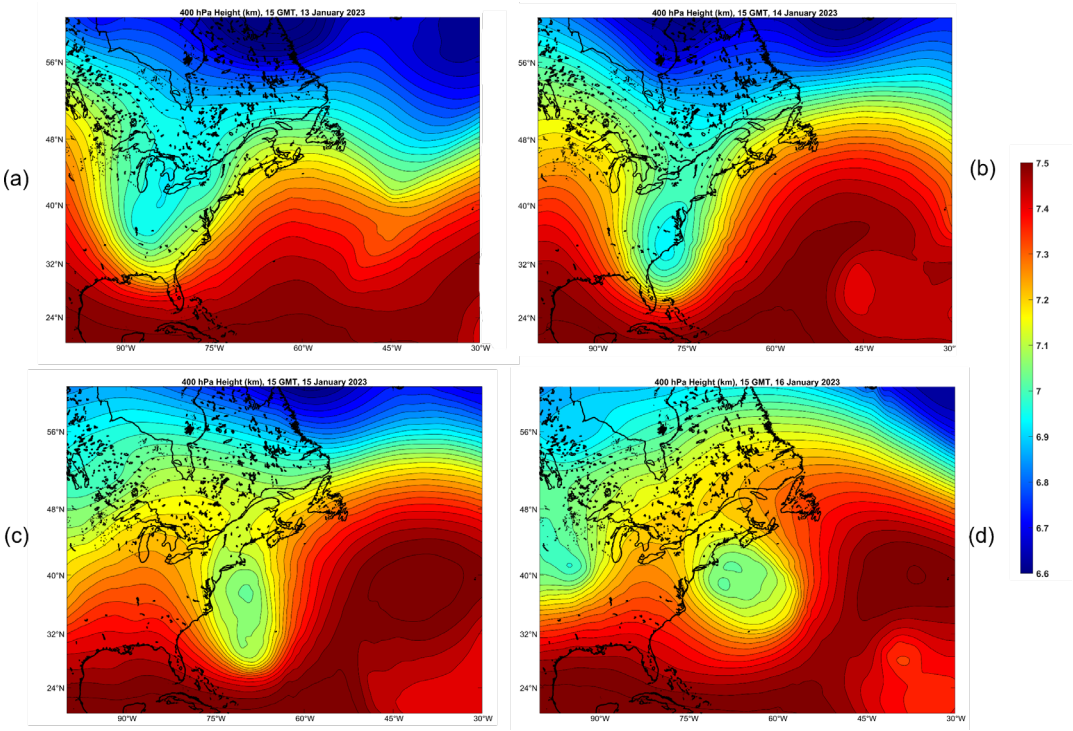

Figure 17: 400 hPa geopotential height (km) at 15:00 GMT on January 13th (a), 14th (b), 15th (c), and 16th (d). From ERA-5 reanalyses.

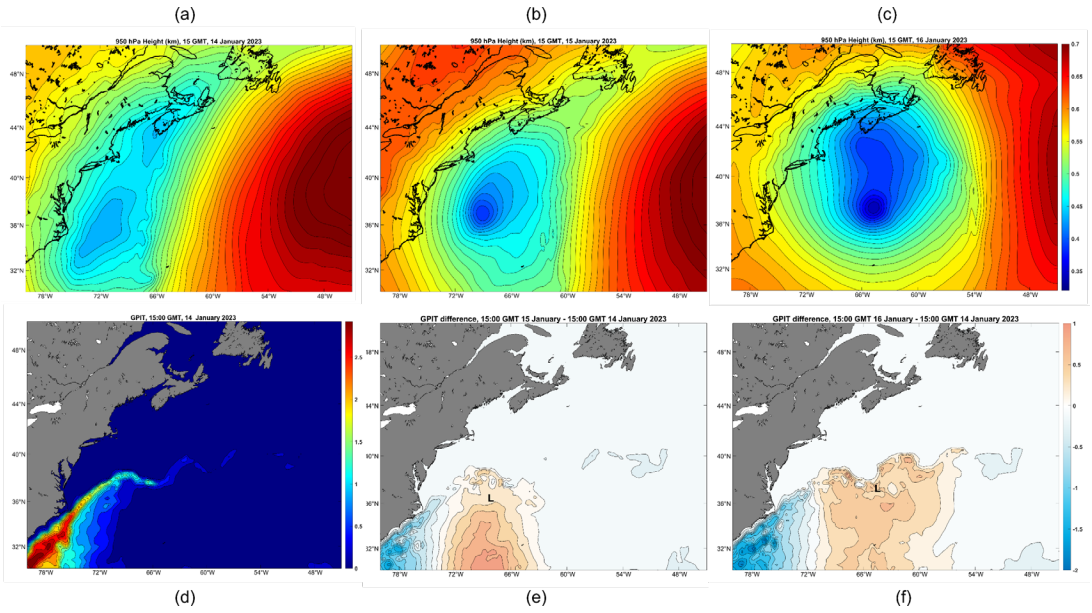

Figure 18: The 950 hPa geopotential height (km) at 15:00 GMT on January 14th (a), 15th (b), 16th (c); the $GPI_{V_{pot}}$ field on January 14th (d). The difference between the $GPI_{V_{pot}}$ of the 15th and 14th is shown in (e) and between the 16th and 14th is shown in (f). Note that the color scales are the same in (e) and (f) and in both panels the "L" shows the position of the surface cyclone at the time of the chart. From ERA-5 reanalyses.

As the upper tropospheric cyclone begins to pull out toward the northeast on the 16th, the surface cyclone intensifies in the region of large $GPI_{V_{pot}}$ south of the Gulf Stream, while the more gradual warming of the surface air in the region of zero north $GPI_{V_{pot}}$ of the Stream yields surface pressure falls, but not as concentrated as in the X-cyclone to the south.

Although the evolution of the upper tropospheric cyclone differs in detail from the previously examined cases, and the sharp gradient of sea surface temperature across the north wall of the Gulfstream clearly plays a role here, in other respects the development of this subtropical cyclone resembles that of other X-cyclones, developing in regions of substantial thermodynamic potential that result from cooling aloft on synoptic time scales.

f. A Kona Storm

Hawaiians use the term “Kona Storm” to describe cold-season storms that typically form west of Hawaii and often bring damaging winds and heavy rain to the islands. The term “Kona” translates to “leeward”, which in this region means the west side of the islands. They may have been first described in the scientific literature by Daingerfield (1921). Simpson (1952) states that Kona Storms possess “cold-core characteristics, with winds and rainfall amounts increasing with distance from the low-pressure center and reaching a maxima at a radius of 200 to 500 mi. However, with intensification, this cyclone may develop warm-core properties, with rainfall and wind profiles bearing a marked resemblance to those of the tropical cyclone.” In general, Simpson’s descriptions of the later stages of some Kona Storms are consistent with their being X-cyclones. But it should be noted that the term is routinely applied to cold-season storms that bring hazardous conditions to Hawaii regardless of whether they have developed warm cores. Here we focus on those that do, providing as a single example the Kona Storm of 19 December 2010. A visible satellite image of this storm is shown in Figure 19.

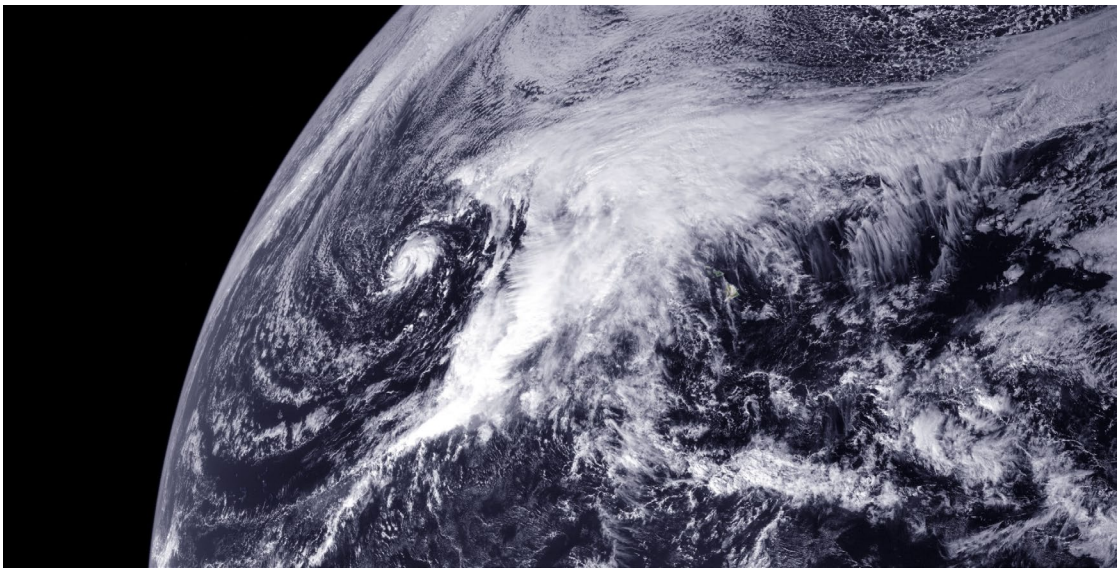

Figure 19: Geostationary satellite visible image showing a Kona Storm at 00 GMT on 19 December 2010. The Kona Storm is the small-scale cyclone left of the major cloud mass.

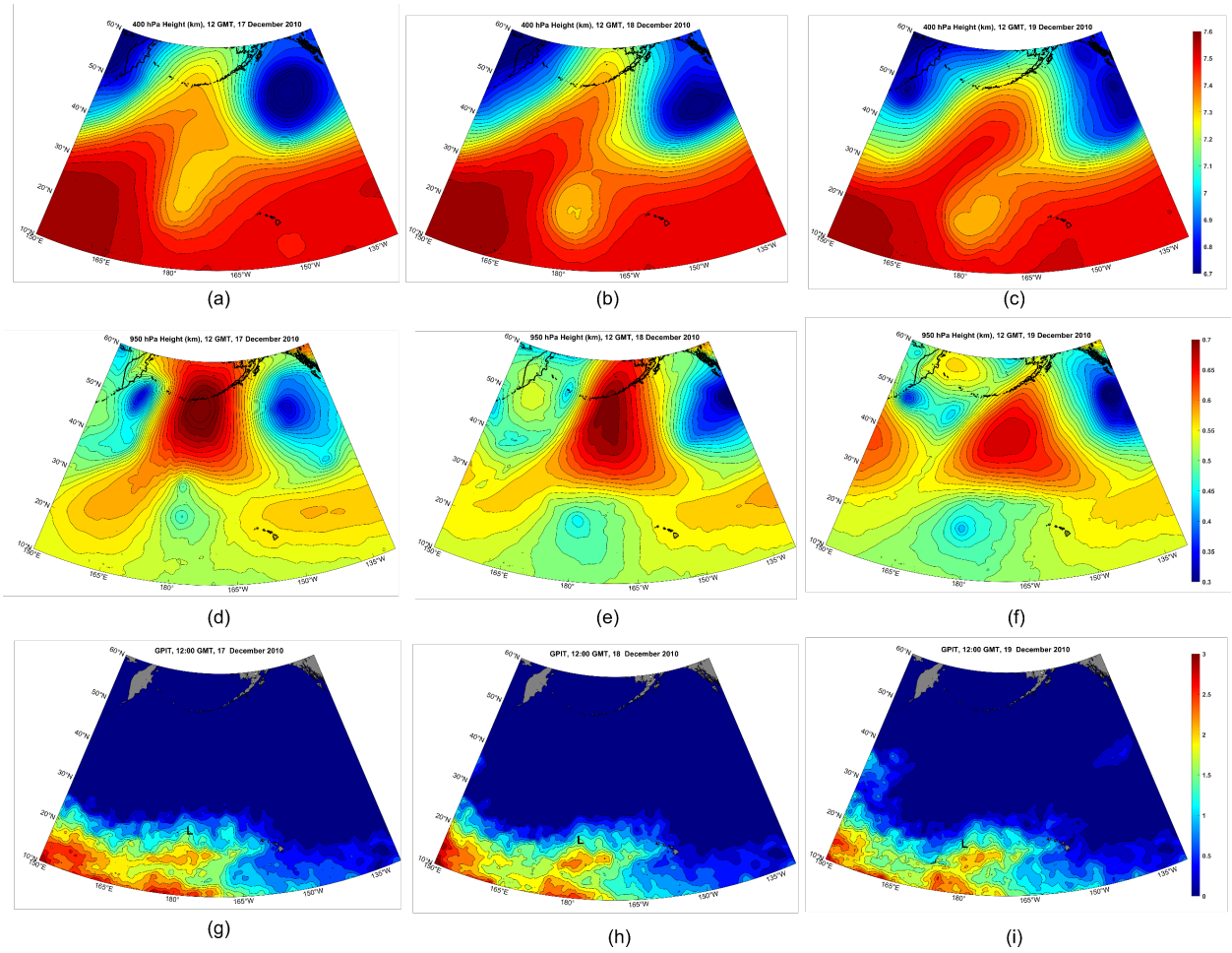

Figure 20: Sequence of 400 hPa geopotential height charts (km; (a)-(c)), 950 hPa geopotential heights (km; (d)-(f)), and $GPI_{V_{pot}}$ ((g)-(i)) at 12:00 GMT on December 17th ((a), (d), (g)), December 18th ((b), (e), (h), and December 19th ((c), (f), (i)) 2010. The "L"s in ((g)-(i)) denote the positions of the 950 hPa cyclone center. From ERA-5 reanalyses.

As with all known X-cyclones, the December 2010 Kona Storm developed under a cold-core cutoff cyclone aloft, as shown in Figure 20. The upper-level cyclone had a long and illustrious history before December 18th, having meandered over a large swath of the central North Pacific. But beginning on December 17th, the cutoff cyclone made a decisive swing southward over waters with higher values of $GPI_{V_{pot}}$. A broad surface cyclone was present underneath the cold pool aloft on all three days, but developed a tight inner core on the 19th as the cold pool slowly drifted over a region of higher thermodynamic potential.

This development more nearly resembles a tropical transition (Bosart and Bartlo 1991; Davis and Bosart 2003, 2004) than a pure X-cyclone, because the upper cutoff cyclone had relatively little effect on the thermodynamic susceptibility to surface flux-driven cyclones. Indeed, this development resulted in a cyclone that was declared Tropical Storm Omeka of 2010. However, other cases of Kona Storms more nearly meet the criterion that X-cyclones form in places and times not climatologically conducive to surface flux-driven cyclones. Figure 21 shows the 950

hPa geopotential height field of the Kona Storm of March, 1951. The storm, at that time, was classified by the Joint Typhoon Warning Center as a tropical cyclone, but the climatological potential intensity there at that time of year could not have supported any tropical cyclone. Figure 21c shows that substantial $GPI_{V_{pot}}$ was associated with a cutoff cyclone in the upper troposphere, making possible the existence of an X-cyclone.

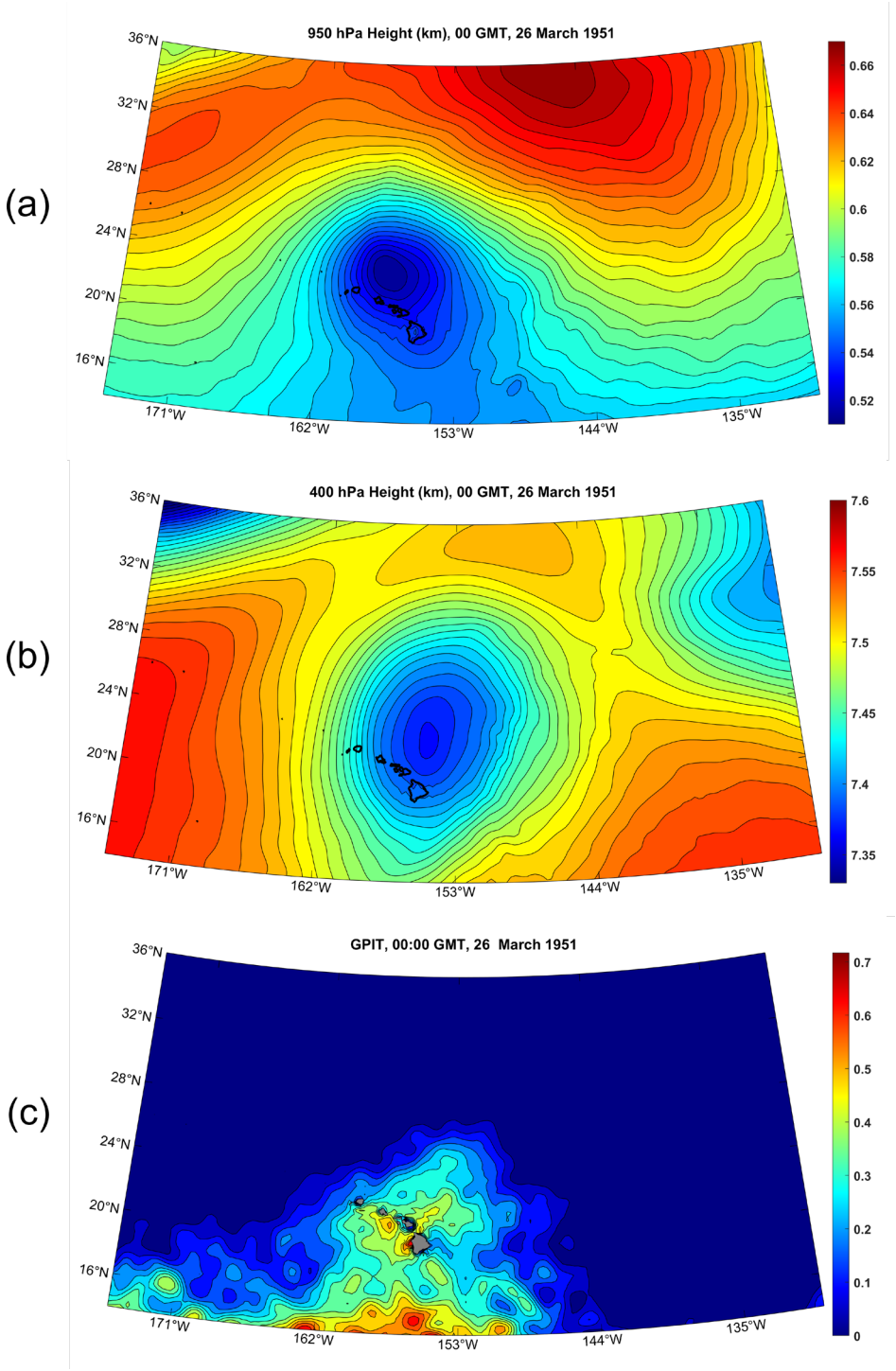

Figure 21: Kona Cyclone of March, 1951. Fields are shown at 00 GMT on 26 March: a): 950 hPa geopotential height (km), b): 400 hPa geopotential height (km), and c): $GPI_{V_{pot}}$.

4. Variations on the Theme

We here are attempting to distinguish a class of cyclone, X-cyclones, from other cyclonic storms by their physics, not by the regions in which they develop. Here we present a case of an actual tropical cyclone in the Mediterranean that we do not identify as an X-cyclone.

a. Cyclone Zorbas

The cyclone known as Zorbas developed just north of Libya on 27 September 2018 and moved northward and then northeastward across the Peloponnese and the Aegean (Figure 22). dissipating in early October. The storm killed several people and did millions of dollars of damage.

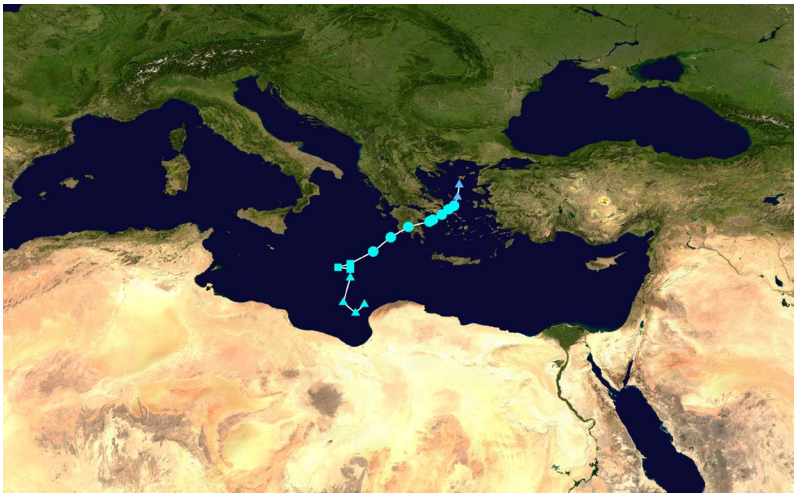

Figure 22: Track of Cyclone Zorbas, from 27 September through 2 October, 2018.

The antecedent potential intensity distribution, on 26 September, is displayed in Figure 23. In much of the Mediterranean, potential intensity was typical of tropical warm pools with values approaching 80 ms^{-1}. As with most medicanes, Zorbas was triggered by an upper tropospheric Rossby wave breaking event (Figure 23), but in this case the cold pool aloft did little to enhance the potential intensity. Zorbas was therefore a classical case of a tropical cyclone resulting from tropical transition (Bosart and Bartlo 1991; Davis and Bosart 2003, 2004) and would not qualify as an X-cyclone. Note that while the approach of the upper-level cyclone did not appreciably alter the potential intensity, it almost certainly humidified the middle troposphere, making genesis somewhat more likely.

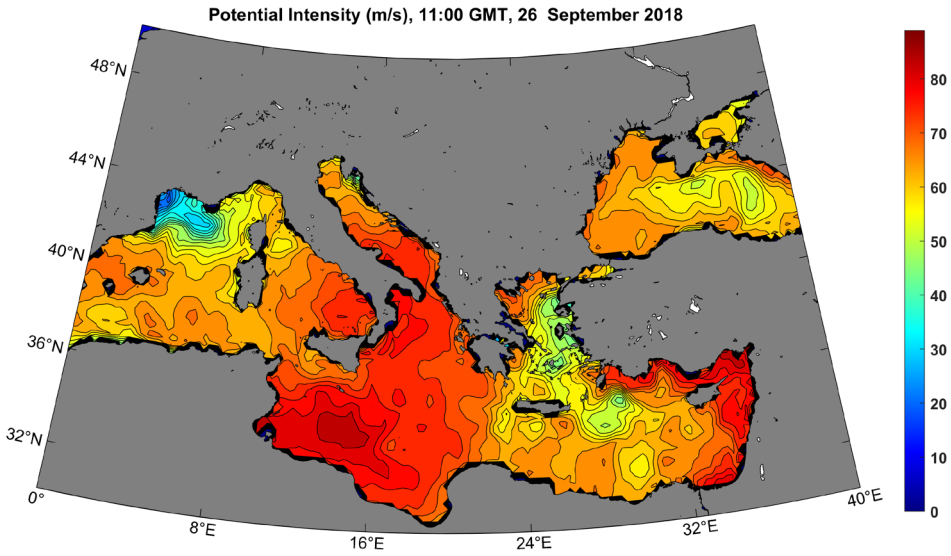

Figure 23: Potential intensity distribution in the Mediterranean and Black Seas, 11 GMT on 26 September 2018.

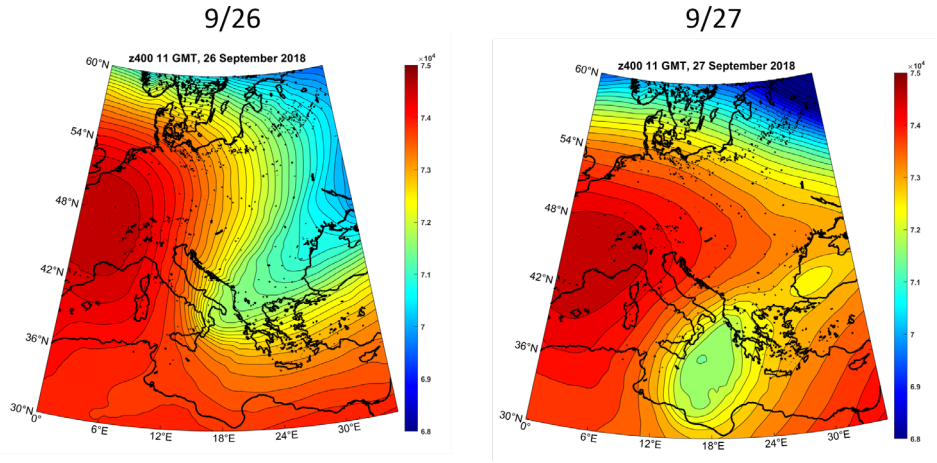

Figure 24: 400 hPa geopotential height (km) at 11 GMT on 26 September (left) and 27 September (right), 2018, from ERA-5 reanalyses.

b. Cyclone Daniel

Cyclone Daniel of 2023 was the deadliest Mediterranean surface flux-driven cyclone in recorded history, with a death toll exceeding 11,000, most of whom perished in floods owing to the catastrophic failure of two dams near Derna, Libya. This flooding was the worst in the recorded history of the African continent. Figure 25 shows the track of Daniel's center and a visible satellite image of the storm as it approached landfall in Libya in shown in Figure 26. Daniel became a surface flux-driven cyclone off the west coast of the Peloponnese on September 5th, made landfall near Benghazi, Libya, on September 10th and dissipated over Egypt on the 12th.

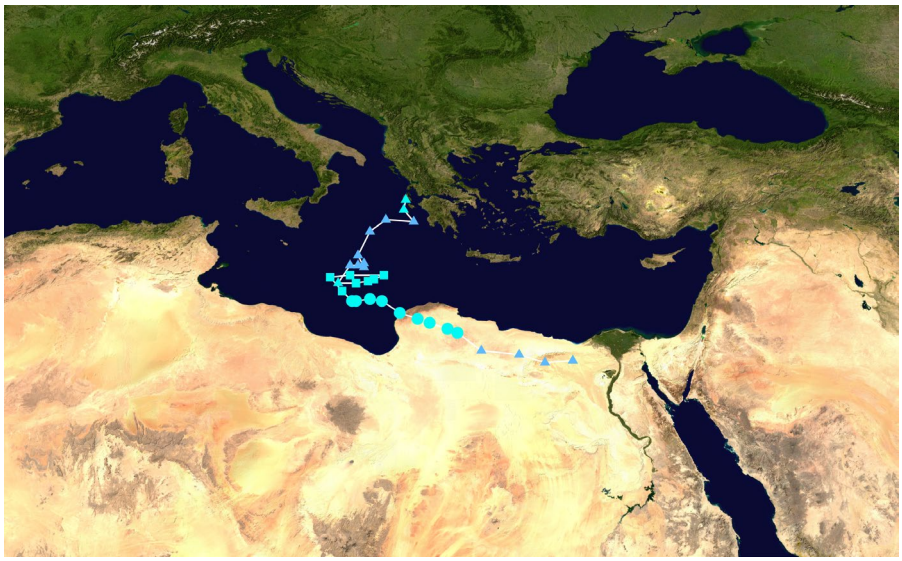

Figure 25: Track of Storm Daniel at 6-hour intervals, beginning September 5th and ending September 12th, 2023.

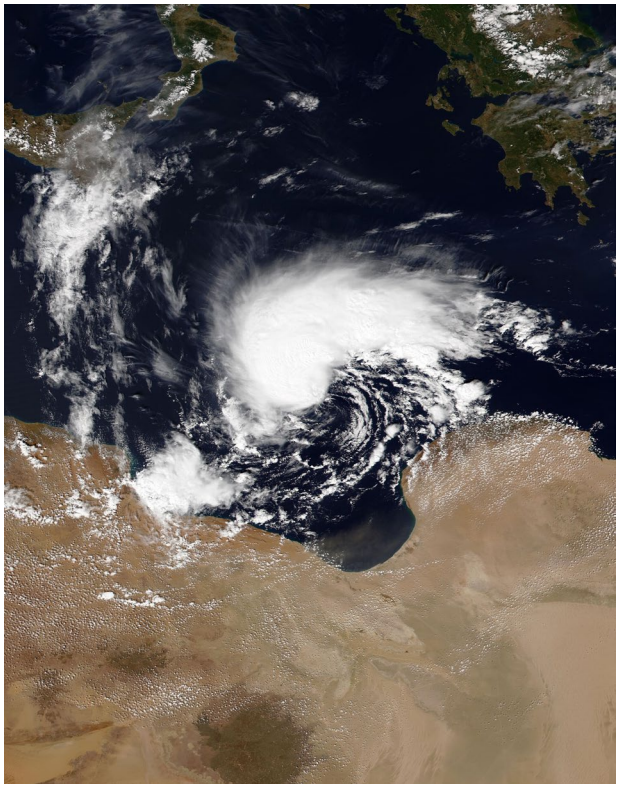

Figure 26: NOAA-20 VIIRS image of Storm Daniel at 12 GMT 9 September 2023, as it approached the Libyan coast.

As with Zorbas, the antecedent potential intensity was high throughout the Mediterranean south and east of Italy and Sicily, and the event was triggered by a Rossby wave breaking event (Figure 27). And as with Zorbas, the cutoff cyclone aloft was not strong enough to have much effect on the potential intensity but acted as a trigger for the tropical cyclone that Daniel became. This was another classic case of tropical transition, and not an X-cyclone.

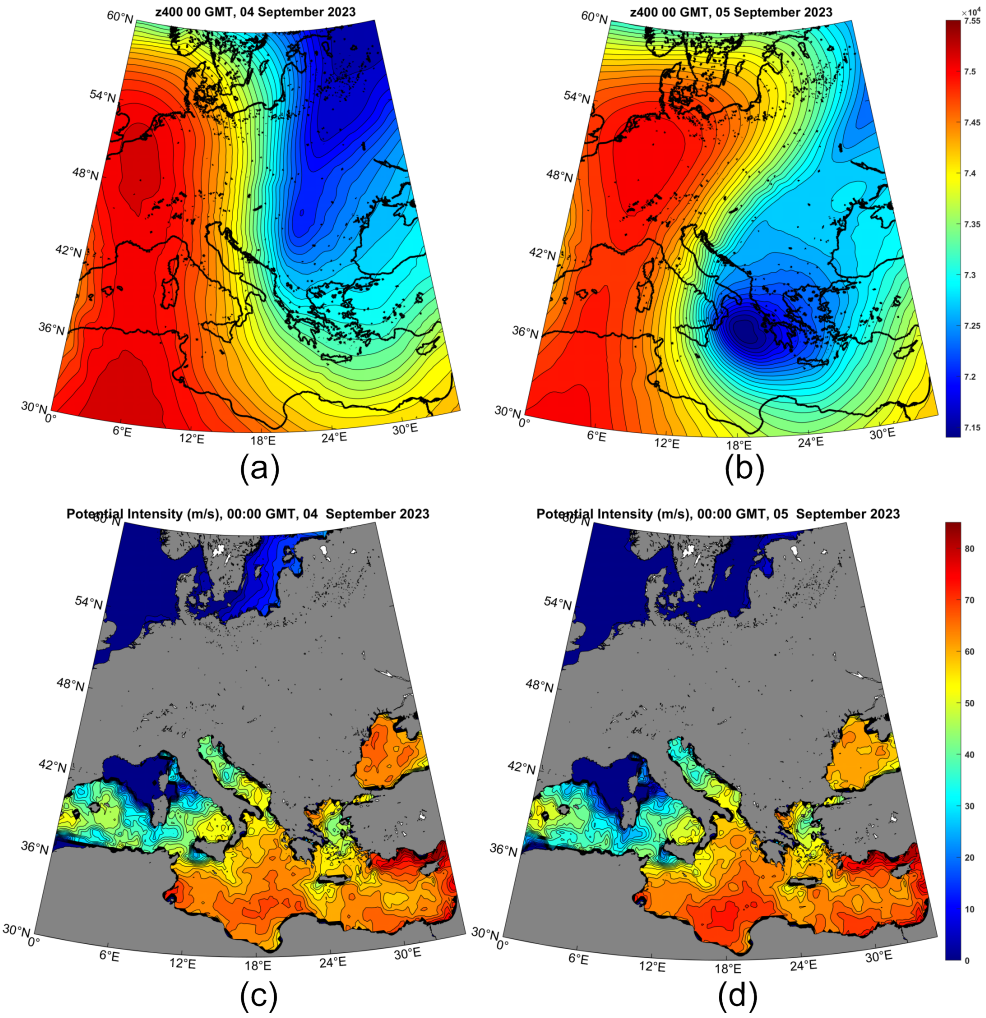

Figure 27: 400 hPa geopotential height (km; (a)-(b)) and potential intensity (ms^{-1}; (c)-(d)) at 00 GMT September 4th ((a) and (c)) and 5th ((b) and (d)), from ERA-5 reanalyses.

Yet Storm Daniel differed from Zorbas in one important respect: As it approached the Libyan coast around September 10th, it came under the influence of strong high-level potential vorticity (PV) advection owing to a mesoscale "satellite" PV mass rotating around the principal upper-level cutoff cyclone (Figure 28). The quasi-balanced forcing associated with the superposition of the high-level PV anomaly with the surface-based warm core probably contributed to Daniel's intensification which, remarkably for a surface flux-driven cyclone, continued after landfall (Tim Hewson, personal communication).

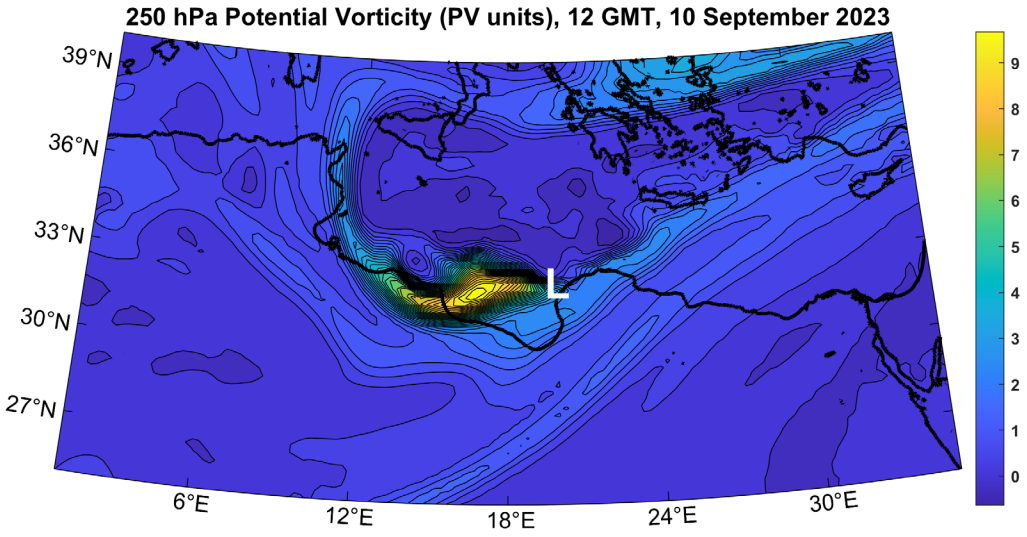

Figure 28: Potential vorticity (PV units, 10^{-6} K kg^{-1} m^2 s^{-1}) at 250 hPa at 12 GMT on 10 September, 2023. The white "L" marks the approximate surface center of Daniel at this time.

5. Summary

We here argue that many of the cyclonic storms called medicanes, polar lows, subtropical cyclones, and Kona storms operate on the same physics and ought to be identified as a single class of storms that we propose to call X-cyclones. Like classical tropical cyclones, these are driven primarily by wind-dependent surface enthalpy (latent and sensible heat) fluxes, but unlike classical TCs, there is little or no climatological thermodynamic potential for the storms, as measured by potential intensity. Rather, the development and approach of strong, cold-core cyclones in the upper troposphere cools and moistens the column through dynamical lifting, giving rise to mesoscale to synoptic scale columns with elevated potential intensity and humidity, and reduced wind shear – ideal embryos for the development of surface flux-driven cyclones.

We do not expect X-cyclones to last as long as classical TCs. In the first place, the conditions that enable such storms are confined in space and transient in time. For example, the cutoff cyclone aloft is often re-absorbed into the main baroclinic flow. In addition, the strong surface enthalpy fluxes that power X-cyclone also increase the enthalpy of the otherwise cold columns in which they form, reducing over time the thermodynamic disequilibrium between the air column and the sea surface. A back-of-the-envelope estimate for the time to destroy the initial thermodynamic disequilibrium is on the order of days. By contrast, even the strongest classical TCs do not warm the tropical troposphere enough to appreciable diminish the large-scale potential intensity of tropical warm pools.

Not all cyclonic storms that have been called polar lows, medicanes, subtropical cyclones, or Kona storms meet our definition of X-cyclone. The literature is full of papers on polar lows that have been traced to something more nearly like classical baroclinic instability acting in an airmass of anomalously low static stability (e.g. Sardie and Warner 1985). Many storms identified as Kona storms because of their location and season, and which developed under cold cyclones aloft, never received much of a boost from surface fluxes and therefore would not be classified as X-cyclones. And, as we described in the last section, two strong Mediterranean cyclones, Zorbas of 2018 and Daniel of 2023, developed in environments of plenty of climatological potential intensity and formed via the tropical transition process.

Synoptic scale processes, like Rossby wave breaking, are essential not only for triggering X-cyclones but for providing conducive thermodynamic and kinematic environments for their development. As such, forecasters must account for both the triggering potential and mesoscale to synoptic scale environmental development in predicting the formation and evolution of X-cyclones. To simulate X-cyclones, NWP models need to make accurate forecasts of baroclinic processes that lead to the formation and humidification of deep cold pools aloft, and be able to handle surface fluxes and other boundary layer processes essential to the formation of surface flux-driven cyclones. And, as with tropical cyclones, coupling to the ocean is essential for accurate intensity prediction.

Finally, we hope that researchers will focus on the essential physics of X-cyclones regardless of where in the world they occur. Casting a broader geographical net will harvest a greater sample of such storms and should lead to more rapid progress in understanding and forecasting them.

References

Bister, M., and K. A. Emanuel, 2002: Low frequency variability of tropical cyclone potential intensity, 1: Interannual to interdecadel variability. *J Geophys Res*, **107**, doi:10.1029/2001JD000776.

Bosart, L. F., and J. A. Bartlo, 1991: Tropical storm formation in a baroclinic environment. *Mon Wea Rev*, **119**, 1979–2013.

Cangliosi, J. P., P. Papin, and J. L. Beven, 2023: *Unnamed tropical storm (AL012023).* https://www.nhc.noaa.gov/data/tcr/AL012023_Unnamed.pdf.

Chavas, D. R., and K. A. Emanuel, 2014: Equilibrium tropical cyclone size in an idealized state of axisymmetric radiative–convective equilibrium. *J Atmos Sci*, **71**, 1663–1680.

Cronin, T. W., and D. R. Chavas, 2019: Dry and Semidry Tropical Cyclones. *J. Atmospheric Sci.*, **76**, 2193–2212, https://doi.org/10.1175/jas-d-18-0357.1.

Daingerfield, L. H., 1921: KONA STORMS. *Mon. Weather Rev.*, **49**, 327–329, https://doi.org/10.1175/1520-0493(1921)49<327:ks>2.0.co;2.

Davis, C. A., and L. F. Bosart, 2003: Baroclinically induced tropical cyclogenesis. *Mon. Weather Rev.*, **131**, 2730–2747, https://doi.org/10.1175/1520-0493(2003)131<2730:BITC>2.0.CO;2.

——, and ——, 2004: The TT problem: Forecasting the tropical transition of cyclones. *Bull. Am. Meteorol. Soc.*, **85**, 1657–1662, https://doi.org/10.1175/BAMS-85-11-1657.

Emanuel, K., 2010: Tropical cyclone activity downscaled from NOAA-CIRES reanalysis, 1908-1958. *J Adv Model Earth Sys*, **2**, 1–12.

Emanuel, K. A., 1986: An air-sea interaction theory for tropical cyclones. Part I: Steady state maintenance. *J Atmos Sci*, **43**, 585–605.

Fita, L., and E. Flaounas, 2018: Medicanes as subtropical cyclones: the December 2005 case from the perspective of surface pressure tendency diagnostics and atmospheric water budget. *Q. J. R. Meteorol. Soc.*, **144**, 1028–1044, https://doi.org/10.1002/qj.3273.

McIntyre, M. E., and T. N. Palmer, 1983: Breaking planetary waves in the stratosphere. *Nature*, **305**, 593–600, https://doi.org/10.1038/305593a0.

Miglietta, M. M., D. Carnevale, V. Levizzani, and R. Rotunno, 2021: Role of moist and dry air advection in the development of Mediterranean tropical-like cyclones (medicanes). *Q. J. R. Meteorol. Soc.*, **147**, 876–899, https://doi.org/10.1002/qj.3951.

Nordeng, T. E., and E. A. D.-:10. 1034/j. 1600-0870. 1992. 00001. x Rasmussen, 1992: A most beautiful polar low. A case study of a polar low development in the Bear Island region. *Tellus A*, **44**, 81–99.

Pytharoulis, I., G. C. Craig, and S. P. Ballard, 1999: Study of the Hurricane-like Mediterranean cyclone of January 1995. *Phys. Chem. Earth Part B Hydrol. Oceans Atmosphere*, **24**, 627–632, https://doi.org/10.1016/S1464-1909(99)00056-8.

Sardie, J. M., and T. T. D.-:10. 1111/j. 1600-0870. 1985. tb00444. x Warner, 1985: A numerical study of the development mechanisms of polar lows. *Tellus A*, **37A**, 460–477.

Schröder, M., and Coauthors, 2023: A combined high resolution global TCWV product from microwave and near infrared imagers - COMBI. https://doi.org/10.5676/EUM_SAF_CM/COMBI/V001.

Simpson, R. H., 1952: Evolution of the Kona storm: A subtropical cyclone. *J. Atmospheric Sci.*, **9**, 24–35, https://doi.org/10.1175/1520-0469(1952)009<0024:EOTKSA>2.0.CO;2.

Tomita, H., and R. Tanaka, 2024: Ocean surface warming and cooling responses and feedback processes associated with polar lows over the Nordic seas. *J. Geophys. Res. Atmospheres*, **129**, e2023JD040460, https://doi.org/10.1029/2023JD040460.

Velez-Pardo, M., and T. W. Cronin, 2023: Large-scale circulations and dry tropical cyclones in direct numerical simulations of rotating Rayleigh-Bénard convection. *J. Atmospheric Sci.*, https://doi.org/10.1175/JAS-D-23-0018.1.

Yanase, W. and co-authors, 2016: Climatology of polar lows over the Sea of Japan using the JRA-55 reanalysis. *J Clim.*, **29**, 419–437.